Microscopic Description of 2α Decay in ^212Po and ^224Ra Isotopes

Mercier, F.; Zhao, J.; Ebran, J.-P.; Khan, E.; Nikšić, Tamara; Vretenar, Dario

Microscopic Description of 2α Decay in ^{212}Po and ^{224}Ra Isotopes

F. Mercier,[1] J. Zhao,[2] J.-P. Ebran,[3,4] E. Khan,[1] T. Nikšić,[5] and D. Vretenar[5]
[1]*IJCLab, Université Paris-Saclay, CNRS/IN2P3, 91405 Orsay Cedex, France*
[2]*Center for Circuits and Systems, Peng Cheng Laboratory, Shenzhen 518055, China*
[3]*CEA, DAM, DIF, F-91297 Arpajon, France*
[4]*Université Paris-Saclay, CEA, Laboratoire Matière en Conditions Extrêmes, 91680 Bruyères-le-Châtel, France*
[5]*Physics Department, Faculty of Science, University of Zagreb, 10000 Zagreb, Croatia*

(Received 2 April 2021; revised 11 May 2021; accepted 8 June 2021; published 2 July 2021)

A microscopic calculation of half-lives for both the α and 2α decays of ^{212}Po and ^{224}Ra is performed, using a self-consistent framework based on energy density functionals. A relativistic density functional and a separable pairing interaction of finite range are used to compute axially symmetric deformation energy surfaces as functions of quadrupole, octupole, and hexadecapole collective coordinates. Dynamical least-action paths are determined, that trace the α and 2α emission from the equilibrium deformation to the point of scission. The calculated half-lives for the α decay of ^{212}Po and ^{224}Ra are in good agreement with data. A new decay mode, the symmetric 2α emission, is predicted with half-lives of the order of those observed for cluster emission.

DOI: 10.1103/PhysRevLett.127.012501

Radioactive decays driven by the strong interaction present a difficult and long-standing nuclear physics problem [1]. Even though the field, initiated by the observation of α decay, is more than hundred years old, not all possible decay modes have been identified. In addition to extensively investigated phenomena, such as the α decay and fission process, more exotic decay modes have been studied, both experimentally and theoretically. For instance, cluster decays [2] and two-proton radioactivity [3,4]. Another intriguing possibility is the spontaneous and simultaneous emission of 2α particles from a heavy nucleus. Although not observed yet, this decay mode has been analyzed in a semimicroscopic approach, in which the 2α decay is considered as a ^{8}Be-like mode [5,6]. The nucleus ^{8}Be is, of course, unstable and decays into two α particles with $T_{1/2} \simeq 10^{-16}$ s. The predicted half-lives for spontaneous 2α decay of heavy nuclei, however, $T_{1/2} \simeq 10^{33}$ years or more, indicate that the experimental detection of this mode is very unlikely.

Alpha, cluster, and fission decay processes have successfully been described with semimicroscopic methods [7,8]. Here, however, we aim to use a fully self-consistent microscopic approach, based on deformation energy surfaces, to analyze the possibility of 2α emission processes in heavy nuclei. When used in the framework of energy density functionals (EDF), such an approach can quantitatively describe cluster decay as, for instance, in Hartree-Fock Bogoliubov calculations with the Gogny energy functional [9,10]. The model that we employ in the present study is based on relativistic EDFs that have very successfully been used to describe nuclear structure phenomena [11], cluster states [12,13], spontaneous and induced fission [14–18], and α decay [19–21].

In particular, in the recent study of Ref. [19], we calculated the half-lives for the recently observed ^{108}Xe $\rightarrow$ ^{104}Te $\rightarrow$ ^{100}Sn α-decay chain. The relativistic density functional DD-PC1 [22] and a separable pairing interaction of finite range were used to compute axially symmetric deformation energy surfaces of ^{104}Te and ^{108}Xe as functions of quadrupole and octupole collective coordinates. Dynamical least-action paths were determined that trace the α-particle emission from the equilibrium deformation to the point of scission. Here, we use the same model to explore α decays and possible 2α decays in the region of heavier nuclei, specifically for the isotopes ^{212}Po and ^{224}Ra. We will show that there is a possibility for the two α particles to be emitted back to back, in a symmetric way, rather than spatially correlated as in a ^{8}Be-like mode. The half-life of the symmetric 2α mode may then be significantly reduced, in some cases to the order of half-lives already observed for cluster decay.

A detailed description of the relativistic Hartree-Bogoliubov (RHB) self-consistent model can be found in Refs. [11,23,24]. Here, it is used to perform constrained calculations of axially symmetric energy surfaces of α emitters, as functions of intrinsic deformation parameters. We then follow the α or 2α emission along a dynamical path L embedded in a multidimensional collective space. For the α emission process, the collective space is three dimensional $(\beta_{20}, \beta_{30}, \beta_{40})$, while for the symmetric 2α emission, because of reflection symmetry, the collective space can be built from the coordinates β_{20} and β_{40}.

The path L is determined by minimizing the action integral [25,26]:

$$S(L) = \int_{s_{\rm in}}^{s_{\rm out}} \frac{1}{\hbar}\sqrt{2\mathcal{M}_{\rm eff}(s)[V_{\rm eff}(s) - E_0]}ds, \quad (1)$$

where $\mathcal{M}_{\rm eff}(s)$ and $V_{\rm eff}(s)$ are the effective collective inertia and potential, respectively. E_0 is the collective ground-state energy, and the integration limits correspond to the classical inner ($s_{\rm in}$) and outer ($s_{\rm out}$) turning points, defined by $V_{\rm eff}(s) = E_0$. In practice the least-action path is built from the inner turning point to the scission point, whose position is determined by monitoring the integrated density distribution, that is, the mass of the emerging fragment. We select the point with emerging fragment mass equal to the mass of the α particle or 2α particles. For the single α emission process, beyond the scission point the configuration with two well separated fragments becomes the lowest energy solution and the energy can be approximated by the classical expression for two uniformly charged spheres:

$$V_{\rm eff}(\beta_3) = e^2\frac{Z_1 Z_2}{R} - Q, \quad (2)$$

where R denotes the distance between the centers of mass of the fragments, and the second term is the experimental Q value. The relation between R and the octupole moment q_{30} is approximated following Eqs. (9) and (10) of Ref. [9]

$$q_{30} = f_3 R^3, \quad (3)$$

with

$$f_3 = \frac{A_1 A_2}{A}\frac{(A_1 - A_2)}{A}, \quad (4)$$

and $\beta_{30} = 4\pi q_{30}/3AR^3$. The corresponding effective collective mass reads

$$\mathcal{M}_{\rm eff} = \frac{\mu}{9 q_{30}^{4/3} f_3^{2/3}}, \quad (5)$$

where $\mu = m_n A_1 A_2/(A_1 + A_2)$ is the reduced mass of the two fragments, and m_n denotes the nucleon mass [9]. Thus the path involved in the action integral of Eq. (1) consists of the least-action path from $s_{\rm in}$ to scission, and the energy surface is approximated by the Coulomb potential from scission to $s_{\rm out}$ [9]. The α-decay half-life is calculated as $T_{1/2} = \ln 2/(nP)$, where n is the number of assaults on the potential barrier per unit time [27–30], and P is the barrier penetration probability in the Wentzel–Kramers–Brillouin approximation

$$P = \frac{1}{1 + \exp[2S(L)]}. \quad (6)$$

We choose $E_0 = 1$ MeV in Eq. (1) for the value of the collective ground-state energy. For the vibrational frequency $\hbar\omega = 1$ MeV, the corresponding value of n is $10^{20.38}$ s^{-1} [9,31].

The effective inertia in Eq. (1) is computed from the multidimensional collective inertia tensor $\mathcal{M}$ [25,27–30]

$$\mathcal{M}_{\rm eff}(s) = \sum_{ij}\mathcal{M}_{ij}\frac{dq_i}{ds}\frac{dq_j}{ds}, \quad (7)$$

where $q_i(s)$ denotes the collective coordinate as a function of the path's length. The collective inertia tensor is calculated in the perturbative cranking approximation (see Ref. [14] and references cited therein)

$$\mathcal{M} = \hbar^2 M_{(1)}^{-1} M_{(3)} M_{(1)}^{-1}, \quad (8)$$

where

$$[M_{(k)}]_{ij} = \sum_{\mu\nu}\frac{\langle 0|\hat{q}_i|\mu\nu\rangle\langle\mu\nu|\hat{q}_j|0\rangle}{(E_\mu + E_\nu)^k}. \quad (9)$$

The two-quasiparticle nucleon wave functions are denoted by $|\mu\nu\rangle$, and E_μ and E_ν are the corresponding quasiparticle energies. $\hat{q}$ denotes the multipole operators that describe the collective degrees of freedom. The effective collective potential $V_{\rm eff}$ is calculated by subtracting the vibrational zero-point energy (ZPE) from the total RHB deformation energy. The zero-point energy is computed using the Gaussian overlap approximation [29,30,32,33],

$$E_{\rm ZPE} = \frac{1}{4}{\rm Tr}[M_{(2)}^{-1} M_{(1)}]. \quad (10)$$

The microscopic self-consistent solutions of the constrained RHB equations, that is, the single-quasiparticle energies and wave functions on the entire energy surface, provide the microscopic input for the calculation of both the collective inertia and zero-point energy. In the present study the RHB equations are solved by expanding the nucleon spinors in the basis of an axially symmetric harmonic oscillator with $N_f = 20$ ($N_g = N_f + 1$) major oscillator for the large (small) component of the Dirac spinor. The technical details of the solution of the constrained RHB equations can be found in Refs. [14,34]. The self-consistent calculations of deformation energy surfaces are based on the DD-PC1 [22] relativistic functional in the particle-hole channel, and a separable pairing interaction of finite range [35]. The original strength parameters of the pairing force were adjusted to reproduce the pairing gap in nuclear matter as calculated with the D1S parametrization of the Gogny force [35,36]. Here, we have fine-tuned the neutron and proton pairing strengths to reproduce the empirical pairing gaps of the isotope ^{224}Ra. Compared to the original values, this leads to an increase of the neutron

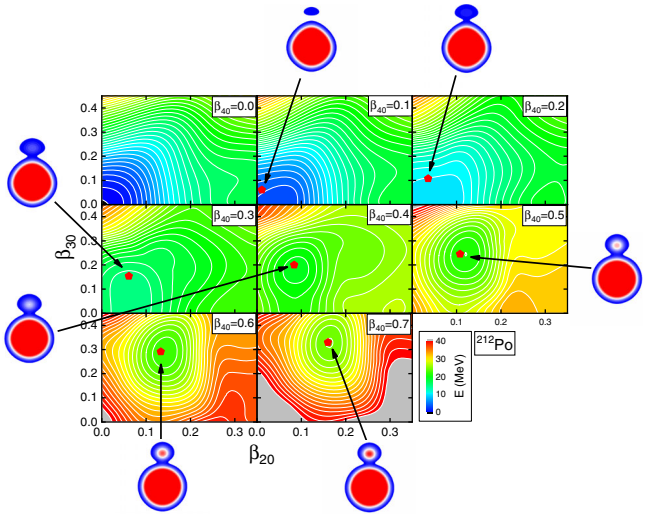

FIG. 1. Deformation energy surface of ^{212}Po in the quadrupole-octupole axially symmetric plane, for selected values of the hexadecapole deformation β_{40}. Calculations are performed using the RHB model based on the DD-PC1 functional and a separable pairing interaction. Contours join points on the surface with the same energy and red circles indicate the points on the dynamical (least-action) path for α emission. The insets display the intrinsic nucleon densities at selected points on the dynamical path.

and proton pairing strengths by 9% and 12%, respectively. This modification of the pairing strength is consistent with the conclusions of the recent global study of the separable pairing interaction, when used with relativistic energy density functionals [37].

To test the model in the region of heavy nuclei, we will first consider the case of the well known α emitter ^{212}Po. Figure 1 displays the deformation energy surface of ^{212}Po in the (β_{20}, β_{30}) plane for several values of the hexadecapole deformation β_{40}. One notices that, for deformations $\beta_{40} \geq 0.5$ and $(\beta_{20}, \beta_{30}) \simeq (0.15, 0.3)$, a pronounced minimum develops on the deformation energy surface at approximately 25 MeV above the equilibrium minimum. The red dots in each panel indicate the points on the dynamical (least-action) path for α emission, and the insets display the corresponding intrinsic nucleon densities along the path, starting from the equilibrium deformation up to the scission point. This point is determined by a discontinuity of β_{40} at the energy minimum. The dimensionless action calculated along the dynamical path up to the scission point is 7.07. The density distribution at the scission point clearly shows the formation of a small cluster of nucleons, and we have verified that the integrated density of this cluster is four nucleons. Beyond the scission point, the dynamics between the two fragments is determined by the Coulomb repulsion [9] and we have calculated the value of 9.46 for the corresponding contribution to the dimensionless action. Therefore, the predicted alpha half-live is $T_\alpha = 0.6$ μs, to be compared with the experimental value of 0.3 μs.

In the case of ^{224}Ra, the scission point for α decay is located at $(\beta_{20}, \beta_{30}, \beta_{40}) \simeq (0.15, 0.31, 0.68)$. The contribution to the dimensionless action along the path up to the scission point is 9.96, and from the scission point to s_{out} 20.50. This leads to the predicted α half-live of 9.5 days, in qualitative agreement with the experimental value of 3.6 days.

The emission of two α particles from a nucleus can occur in several ways. In addition to the obvious sequential 2α process, there have also been some predictions [38], and detection [39] of 2α particles emitted during fission. The ^{8}Be cluster emission [7] has also been predicted, and this process should lead to a 2α state because of the resonant nature of ^{8}Be ($Q_\alpha = 92$ keV).

The process of direct spontaneous emission of two α particles from a nucleus is different. There have only been a few analyses of spontaneous 2α decays: it has been discussed in Ref. [5], and recently a possible experimental investigation has been considered in Ref. [6]. In these studies, the corresponding half-life is approximated by that of the ^{8}Be cluster emission, leading to very long half-lives, of the order of $\log T[s] \simeq 50$ to 100, typically.

A microscopic self-consistent calculation can provide complementary insight on the direct 2α decay process. Here, we will show that the two α particles can be emitted back to back, in a symmetric way, rather than in a ^{8}Be-like mode. The half-life of the symmetric 2α mode may be significantly reduced compared to those of ^{8}Be cluster emission discussed above.

A necessary condition for direct 2α spontaneous emission is a positive Q value. A simple calculation leads to

$$Q_{2\alpha} = Q_{\alpha 1} + Q_{\alpha 2} + \Delta E, \tag{11}$$

where $Q_{\alpha 1,2}$ are the Q values for the α decay of the parent and daughter nuclei, respectively. ΔE is the excitation energy difference between the sum of the one of the daughter and the granddaughter nuclei in the one α decay, and the one of the granddaughter nucleus in the 2α decay. In the following, we consider, for simplicity, α or 2α transitions involving only the ground states of the daughter or granddaughter nuclei (that is, $\Delta E = 0$).

Figure 2 displays a global survey of possible candidates for 2α decay, that is, a map of $N > 50$ and $Z > 50$ nuclei with positive $Q_{2\alpha}$, computed from the available experimental masses [40]. A large number of nuclei are possible candidates for 2α emission, especially "north" of the valley of stability, and this is also the case for single α emission. Of course, the main problem in detecting a possible 2α mode is its extremely low probability. For instance, much shorter β-decay lifetimes for most of these nuclei prevent the experimental detection of the α decay modes. It is then relevant to consider nuclei for which one of the sequential single-α decays is energetically forbidden. Such nuclei are also shown in Fig 2. If the half-life of the first daughter

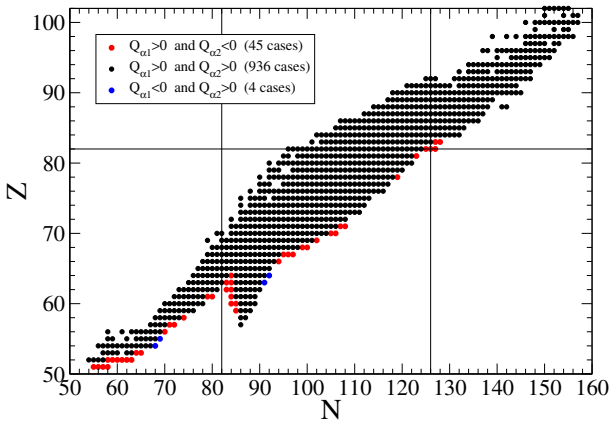

FIG. 2. $N > 50$ and $Z > 50$ nuclei with $Q_{2\alpha} > 0$, computed from the experimental masses [40].

nucleus is long enough, the risk of confusing sequential and direct 2α decays is low [6]. Therefore, the main experimental issue is the very long half-life (low probability) to separate the 2α decay signals from the background. Note, however, that this is also the case for observed cluster radioactivity, with partial half-lives in the range from 10^{11} to 10^{26} seconds, and branching ratios with respect to the dominant α decay between 10^{-9} and 10^{-16}. The emission of clusters ranging from ^{14}C to ^{34}Si has been observed in the actinide region, from ^{221}Fr to ^{242}Cm [7].

In this study we describe the symmetric 2α decay using the quadrupole and hexadecapole collective coordinates. Figure 3 displays the axially symmetric energy surface of ^{224}Ra, as a function of the quadrupole and hexadecapole intrinsic deformations. The dynamic path for 2α emission starting from the equilibrium deformation and up to the scission point located at $(\beta_{20}, \beta_{40}) \simeq (0.28, 1.30)$, is traced by the dashed curve. The corresponding contribution to the dimensionless action of Eq. (1) is $\approx$16. To calculate the contribution of the action from the scission point to the outer turning point s_{out}, we consider the superposition of each alpha + nucleus Coulomb interaction system, namely:

$$V_{\text{eff}}(\beta_2) = 2e^2 \frac{Z_1 Z_2}{R} - Q_{2\alpha}, \tag{12}$$

where R represents the distance between the centers of mass of the fragments (the index 1 refers to the heavy fragment, and 2 to the α). The approximate relation between R and the quadrupole moment is

$$q_{20} = 2A_2 R. \tag{13}$$

The corresponding effective collective mass reads

$$\mathcal{M}_{\text{eff}} = \frac{\mu}{8A_2 q_{20}}, \tag{14}$$

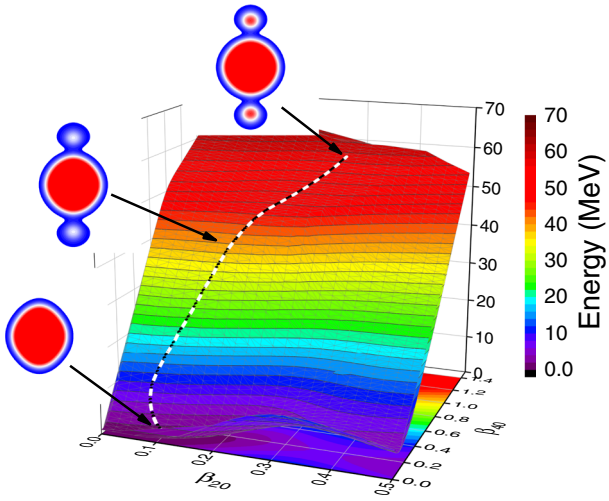

FIG. 3. Reflection symmetric deformation energy surface of ^{224}Ra in the quadrupole-hexadecapole axially symmetric plane. Calculations are carried out using the RHB model based on the DD-PC1 functional, and separable pairing interaction. The black and white dashed curve denotes the dynamical (least-action) path for 2α emission from equilibrium deformation to scission, and the insets display the intrinsic nucleon densities for three selected points on the path.

where $\mu = m_n A_2/2$ is the reduced mass of the $(2\alpha + \text{heavy})$ fragments. This yields a scission to 2α emission action of 23.89. The predicted 2α half-life is $\log T_{2\alpha}[s] = 14.24$, which is much shorter than the ^{8}Be-like emission half-life $\log T_{2\alpha}[s] = 27.87$, calculated using the semiempirical model for cluster decay of Ref. [41]. We have obtained a similar symmetric 2α decay half-life (to within one order of magnitude) with few other standard relativistic energy density functionals. It could, therefore, be interesting to reconsider the cluster detection experiment for this nucleus, aiming to detect two α clusters in coincidence at 180°. The insets in Fig. 3 display the intrinsic nucleon densities for three selected points on

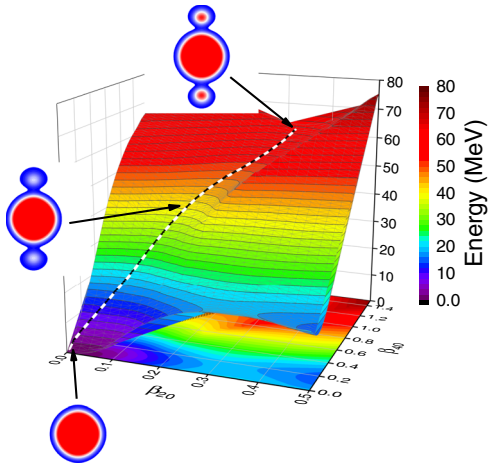

FIG. 4. Same as in the caption to Fig. 3 but for ^{212}Po.

the 2α emission dynamic path. The 2α configuration is clearly visible for the configuration at the scission point.

The symmetric 2α emission mode is, of course, predicted not only in ^{224}Ra. In ^{212}Po, for instance, as shown in Fig. 4, the scission point is located at $(\beta_{20}, \beta_{40}) \simeq (0.32, 1.46)$. The dynamical path shows a pattern similar to the ^{224}Ra case. The contribution to the dimensionless action (1) up to the scission point is 15.56, while the contribution from the scission point to 2α emission is 29.22. The predicted symmetric 2α half-life for ^{212}Po is $\log T_{2\alpha}[s] = 18.36$, to be compared with the much longer half-life for the ^{8}Be decay channel $\log T_{2\alpha}[s] = 38.82$ [41].

In summary, we have applied the self-consistent mean-field framework based on the relativistic DD-PC1 energy density functional and separable pairing interaction, to analyze single α and double α emission processes in ^{212}Po and ^{224}Ra. These decay modes involve different collective coordinates and are characterized with half-lives that differ by orders of magnitude, from 10^{15} s (2α emission) to days or microseconds (α emission). For the possible symmetric 2α decay process, in which the two α particles are emitted in opposite directions, half-lives of the order of those detected for already observed cluster decay modes (from ^{14}C to ^{34}Si) are predicted. For the two examples considered in the present study, these half-lives are many orders of magnitude shorter than those of the ^{8}Be decay channel. The back-to-back decay feature could be used to detect this mode by α detectors in coincidence at 180°.

This work has been supported in part by the QuantiXLie Centre of Excellence, a project cofinanced by the Croatian Government and European Union through the European Regional Development Fund—the Competitiveness and Cohesion Operational Programme (KK.01.1.1.01.0004) and the Croatian Science Foundation under the project Uncertainty quantification within the nuclear energy density framework (IP-2018-01-5987). J. Z. acknowledges support by the National Natural Science Foundation of China under Grants No. 12005107 and No. 11790325. J.-P. E., E. K., and F. M. thank R. Lasseri for fruitful discussions.

[1] D. S. Delion, Lect. Notes Phys. **819**, 1 (2010), https://link-springer-com.proxy.scd.u-psud.fr/book/10.1007/978-3-642-14406-6.
[2] H. J. Rose and G. A. Jones, Nature (London) **307**, 245 (1984).
[3] J. Giovinazzo, B. Blank, M. Chartier, S. Czajkowski, A. Fleury *et al.*, Phys. Rev. Lett. **89**, 102501 (2002).
[4] M. Pfützner *et al.*, Eur. Phys. J. A **14**, 279 (2002).
[5] D. N. Poenaru and M. Ivascu, J. Phys. Lett. **46**, 591 (1985).
[6] V. I. Tretyak, arXiv:2102.12005.
[7] D. N. Poenaru and W. Greiner, Lect. Notes Phys. **818**, 1 (2010).
[8] R. K. Gupta, Lect. Notes Phys. **818**, 223 (2010).
[9] M. Warda and L. M. Robledo, Phys. Rev. C **84**, 044608 (2011).
[10] M. Warda, A. Zdeb, and L. M. Robledo, Phys. Rev. C **98**, 041602(R) (2018).
[11] D. Vretenar, A. V. Afanasjev, G. A. Lalazissis, and P. Ring, Phys. Rep. **409**, 101 (2005).
[12] P. Marević, J. P. Ebran, E. Khan, T. Nikšić, and D. Vretenar, Phys. Rev. C **97**, 024334 (2018).
[13] P.Marević, J. P. Ebran, E. Khan, T. Nikšić, and D. Vretenar, Phys. Rev. C **99**, 034317 (2019).
[14] J. Zhao, B.-N. Lu, T. Nikšić, and D. Vretenar, Phys. Rev. C **92**, 064315 (2015).
[15] J. Zhao, B.-N. Lu, T. Nikšić, D. Vretenar, and S.-G. Zhou, Phys. Rev. C **93**, 044315 (2016).
[16] H. Tao, J. Zhao, Z. P. Li, T. Nikšić, and D. Vretenar, Phys. Rev. C **96**, 024319 (2017).
[17] J. Zhao, T. Nikšić, D. Vretenar, and S.-G. Zhou, Phys. Rev. C **99**, 014618 (2019).
[18] J. Zhao, J. Xiang, Z.-P. Li, T. Nikšić, D. Vretenar, and S.-G. Zhou, Phys. Rev. C **99**, 054613 (2019).
[19] F. Mercier, J. Zhao, R.-D. Lasseri, J. P. Ebran, E. Khan, T. Nikšić, and D. Vretenar, Phys. Rev. C **102**, 011301(R) (2020).
[20] J. P. Ebran, E. Khan, R. D. Lasseri, and D. Vretenar, Phys. Rev. C **97**, 061301(R) (2018).
[21] J. P. Ebran, E. Khan, and R. D. Lasseri, J. Phys. G **48**, 025106 (2021).
[22] T. Nikšić, D. Vretenar, and P. Ring, Phys. Rev. C **78**, 034318 (2008).
[23] J. Meng, *Relativistic Density Functional for Nuclear Structure* (World Scientific, Singapore, 2016).
[24] J. P. Ebran, in *Energy Density Functional Methods for Atomic Nuclei* (IOP Publishing, Bristol, 2019).
[25] M. Brack, J. Damgaard, A. S. Jensen, H. C. Pauli, V. M. Strutinsky, and C. Y. Wong, Rev. Mod. Phys. **44**, 320 (1972).
[26] T. Ledergerber and H.-C. Pauli, Nucl. Phys. **A207**, 1 (1973).
[27] A. Baran, Phys. Lett. **76B**, 8 (1978).
[28] A. Baran, K. Pomorski, A. Lukasiak, and A. Sobiczewski, Nucl. Phys. **A361**, 83 (1981).
[29] J. Sadhukhan, K. Mazurek, A. Baran, J. Dobaczewski, W. Nazarewicz, and J. A. Sheikh, Phys. Rev. C **88**, 064314 (2013).
[30] J. Sadhukhan, J. Dobaczewski, W. Nazarewicz, J. A. Sheikh, and A. Baran, Phys. Rev. C **90**, 061304(R) (2014).
[31] D. L. Hill and J. A. Wheeler, Phys. Rev. **89**, 1102 (1953).
[32] A. Staszczak, A. Baran, and W. Nazarewicz, Phys. Rev. C **87**, 024320 (2013).
[33] A. Baran, A. Staszczak, J. Dobaczewski, and W. Nazarewicz, Int. J. Mod. Phys. E **16**, 443 (2007).
[34] B.-N. Lu, J. Zhao, E.-G. Zhao, and S.-G. Zhou, Phys. Rev. C **89**, 014323 (2014).
[35] Y. Tian, Z. Y. Ma, and P. Ring, Phys. Lett. B **676**, 44 (2009).
[36] J.-F. Berger, M. Girod, and D. Gogny, Comput. Phys. Commun. **63**, 365 (1991).
[37] S. Teeti and A. V. Afanasjev, Phys. Rev. C **103**, 034310 (2021).

[38] D. N. Poenaru, W. Greiner, J. H. Hamilton, A. V. Ramayya, E. Hourany, and R. A. Gherghescu, Phys. Rev. C **59**, 3457 (1999).

[39] F. Gönnewein, M. Mutterer, and Y. Kopatch, Europhysics News **36**, 11 (2005).

[40] A. H. Wapstra, G. Audi, and C. Thibault, Nucl. Phys. **A729**, 129 (2003).

[41] D. N. Poenaru, Y. Nagame, R. A. Gherghescu, and W. Greiner, Phys. Rev. C **65**, 054308 (2002).